# Transmissibility-function-based structural damage detection with tetherless mobile sensors

Xiaohua Yi, Dapeng Zhu, Yang Wang
*School of Civil and Environmental Engineering, Georgia Institute of Technology, Atlanta, GA 30332*

Jiajie Guo, Kok-Meng Lee
*School of Mechanical Engineering, Georgia Institute of Technology, Atlanta, GA 30332*

ABSTRACT: In order to reduce the cost and inaccuracy associated with human inspection, prototype mobile sensors are developed for the damage detection of steel structures. The individual mobile sensing nodes consist of magnet-wheeled robots that are capable of autonomously maneuvering on ferromagnetic surfaces. Upon moving to a new measurement location, the mobile sensing node can collect structural sensor data and wirelessly transmit data back to a computer. The performance of the mobile sensing nodes is validated in laboratory experiments. Transmissibility function analysis is adopted for detecting structural damage using the data collected by mobile sensing nodes. This preliminary work is expected to spawn transformative changes of using mobile sensors for future structural health monitoring.

## 1 INTRODUCTION

Civil structures may deteriorate rapidly due to various adverse operational and environmental conditions. For example, 12.1% of the bridges in the United States were categorized as structurally deficient and 14.8% were categorized as functionally obsolete, according to the 2009 ASCE Report Card for America's Infrastructure. The American Association of State Highway and Transportation Officials (AASHTO) estimated in 2008 that it would cost roughly $140 billion to repair every deficient bridge in the United States (AASHTO 2008).

To efficiently utilize limited resources and achieve condition-based maintenance, many vibration-based methods have been developed for structural damage detection (Doebling et al. 1998). Among these methods, transmissibility function analysis has attracted considerable attention because of its effectiveness in identifying damage using output data only. For the damage detection of a composite beam, Zhang et al. (1999) used translational and curvature transmissibility functions to calculate damage indicators and successfully located damage. In the lab experiments, a piezoceramic patch actuator is used to excite the cantilever beam. The experimental results showed that the performance of determining damage locations varies with the frequency range adopted in the transmissibility function analysis. Transmissibility function analysis was also applied to the damage detection, localization, and quantification for linear and nonlinear structures by Johnson and Adams (2002). Johnson et al. (2004) described the application with a three-story building and a rotorcraft fuselage. In these two references, an electromagnetic shaker was attached to the structure for applying excitation, and the structural damage was correctly located. In addition, the effects of operational and environmental variability on the transmissibility function analysis were analyzed by Kess and Adams (2007). Their work suggested that the accuracy of damage detection based on transmissibility function analysis could be improved by identifying specific frequency ranges that are more sensitive to damage and immune to sources of uncertainties. Most recently, Devriendt and Guillaume (2008) concluded that arbitrary forces could be used to perform the transmissibility-function-based operational modal analysis, as long as the structure is persistently excited in the frequency range of interest.

As the input for transmissibility function analysis, structural vibration data needs to be collected by a data acquisition system. To reduce the instrumentation time and cost of conventional cable-based data acquisition systems, wireless technologies have been widely explored in the past decade for structural health monitoring (Lynch and Loh 2006). Akyildiz et al. (2002) predicted that as a transformative change to wireless sensing, the next revolution in sensor networks would be mobile sensing systems that contain individual mobile sensing nodes. Each mobile sensing node can explore its surroundings and exchange information with its peers through wireless communication. Using limited number of sensing nodes, a mobile sensing system offers meas-

urement data with adaptive spatial resolutions. In our previous research, Lee et al. (2009) introduced the development and implementation of a flexonic mobile sensing node, which is capable of attaching/detaching sensors onto/from the structural surface. The flexonic mobile sensing node has the potential to fulfill functions of negotiating in complex steel structures with narrow sections, high abrupt angle changes, as well as firmly attaching an accelerometer onto the structure. Laboratory experiments demonstrated that data collected by a reference static sensor matched well with the data collected by a flexonic mobile sensing node. Guo et al. (2009) conducted further analysis and numerical simulations regarding the compliant mechanism of the flexure-based mobile sensing node.

In this study, we validate the damage detection ability of the flexonic mobile sensing nodes using transmissibility function analysis. Section 2 summarizes the formulation of transmissibility function analysis. In Section 3, design and implementation of the flexure-based mobile sensing node are presented. Section 4 first describes the laboratory experimental setup. Two mobile sensing nodes, each carrying an accelerometer, are adopted in the validation experiments. Procedures and results of damage detection using mobile sensor data are then presented. Section 5 summarizes the research and proposes future work.

## 2 TRANSMISSIBILITY FUNCTION THEORY

The equations of motion for an $n$-degree-of-freedom (n-DOF) linear structure can be formulated as:

$$\mathbf{M}\ddot{\mathbf{x}}(t) + \mathbf{C}\dot{\mathbf{x}}(t) + \mathbf{K}\mathbf{x}(t) = \mathbf{f}(t) \tag{1}$$

where $\mathbf{x}(t)$ is the $n\times1$ displacement vector, $\mathbf{M}$ is the $n\times n$ mass matrix, $\mathbf{C}$ is the $n\times n$ viscous damping matrix, $\mathbf{K}$ is the $n\times n$ stiffness matrix, and $\mathbf{f}(t)$ is the $n\times1$ external force vector. If the external force is only applied to the $k$-th DOF, then $\mathbf{f}(t) = \{0_1, 0_2, \ldots, f_k(t), \ldots, 0_n\}^T$ only has one non-zero entry.

Using Fourier transform, Equation (1) can be represented in frequency domain as:

$$\mathbf{X}(\omega) = \mathbf{H}(\omega)\mathbf{F}(\omega) \tag{2}$$

where $\mathbf{H}(\omega) = \mathbf{B}(\omega)^{-1} = (\mathbf{K}-\omega^2\mathbf{M}+\mathrm{i}\omega\mathbf{C})^{-1} = \mathbf{D}(\omega)/\Delta(\omega)$ is the $n\times n$ frequency response function (FRF) matrix, $\mathbf{D}(\omega)$ and $\Delta(\omega)$ are the adjugate matrix and the determinant of the impedance matrix $\mathbf{B}(\omega)$, respectively. Assuming the external force is only applied to the $k$-th DOF, the Fourier transform of the input force vector $\mathbf{f}(t)$ is determined as:

$$\mathbf{F}(\omega) = \{0_1, 0_2, \ldots, F_k(\omega), \ldots, 0_n\}^T \tag{3}$$

The acceleration vector in the frequency domain can be computed from Equation (2) as:

$$\mathbf{A}(\omega) = -\omega^2\mathbf{H}(\omega)\mathbf{F}(\omega) \tag{4}$$

The transmissibility function $T_{ij}(\omega)$ between the output DOF $i$ and reference-output DOF $j$ is defined as the ratio between two frequency spectra $A_i(\omega)$ and $A_j(\omega)$. Letting $\mathbf{h}_i(\omega)$ be the $i$-th row of $\mathbf{H}(\omega)$, then the transmissibility function $T_{ij}(\omega)$ can be calculated as:

$$T_{ij}(\omega) = \frac{A_i(\omega)}{A_j(\omega)} = \frac{-\omega^2\mathbf{h}_i(\omega)\mathbf{F}(\omega)}{-\omega^2\mathbf{h}_j(\omega)\mathbf{F}(\omega)} = \frac{\mathbf{h}_i(\omega)\mathbf{F}(\omega)}{\mathbf{h}_j(\omega)\mathbf{F}(\omega)} \tag{5}$$

Substituting the expression of $\mathbf{F}(\omega)$ (Equation (3)) into Equation (5), then $T_{ij}$ is further simplified as:

$$T_{ij}(\omega) = \frac{H_{ik}(\omega)}{H_{jk}(\omega)} = \frac{D_{ik}(\omega)/\Delta(\omega)}{D_{jk}(\omega)/\Delta(\omega)} = \frac{D_{ik}(\omega)}{D_{jk}(\omega)} \tag{6}$$

where $H_{ik}(\omega)$, $H_{jk}(\omega)$ are entries of the FRF matrix, and $D_{ik}(\omega)$, $D_{jk}(\omega)$ are entries of the adjugate matrix. Note that for one specific pair of DOFs, $i$ and $j$, another approach of formulating the transmissibility function is $T_{ji}(\omega) = H_{jk}(\omega)/H_{ik}(\omega)$. Equation (6) shows that the transmissibility function $T_{ij}$ is more sensitive to the zeros of the frequency response function $H_{jk}(\omega)$. On the other hand, $T_{ji}$ is more sensitive to the zeros of the frequency response function $H_{ik}(\omega)$. Among $T_{ij}(\omega)$ and $T_{ji}(\omega)$, if one approach of calculating the transmissibility function is more susceptible to sensor noise, the other approach can be chosen to reduce the noise influence.

An integral damage indicator ($DI$) between DOFs (i.e. locations) $i$ and $j$ is defined as:

$$DI_{ij} = \frac{\int_{\omega_1}^{\omega_2} \left| \ln\left|T_{ij}^U\right| - \ln\left|T_{ij}^D\right| \right| d\omega}{\int_{\omega_1}^{\omega_2} \left| \ln\left|T_{ij}^U\right| \right| d\omega} \tag{7}$$

where $\omega_1$ and $\omega_2$ are the lower and upper boundaries of the interested frequency span; $|\text{-}|$ denotes the magnitude of a complex or a real number; superscript $U$ represents the undamaged structure and superscript $D$ represents the damaged structure. Accordingly, $T_{ij}^U$ represents the transmissibility function of the undamaged structure, and $T_{ij}^D$ represents the transmissibility function of the damaged structure. The damage indicator is defined in logarithmic coordinate, so that the difference among small numbers has larger influence in the integration. In practice, to reduce the effect of experimental uncertainties, the vibration experiments can be repeated for $N$ times for both undamaged and dam-

aged structures. Then the averaged transmissibility functions are used for calculating the damage indicators:

$$T_{ij}^{U} = \frac{1}{N}\sum_{k=1}^{N}(T_{ij}^{U})_k \tag{8a}$$

$$T_{ij}^{D} = \frac{1}{N}\sum_{k=1}^{N}(T_{ij}^{D})_k \tag{8b}$$

where $(T_{ij}{}^{U})_k$ represents the transmissibility function $T_{ij}$ calculated from the $k$-th repeating test with the undamaged structure, between DOFs $i$ and $j$; $(T_{ij}{}^{D})_k$ represents the transmissibility function $T_{ij}$ calculated from the $k$-th repeating test with the damaged structure, at DOFs $i$ and $j$. If acceleration data is available from the experiments, the transmissibility function from each test is calculated according to Equation (5), as the direct division between the frequency spectra of the acceleration at two DOFs $i$ and $j$.

## 3 FLEXONIC MOBILE SENSING NODE IMPLEMENTATION

Figure 1 shows the flexonic mobile sensing node developed by Lee et al. (2009). The flexonic mobile sensing node consists of three substructures: two 2-wheel cars and the compliant connection beam. Each 2-wheel car contains a body frame, motors, batteries, a wireless sensing unit, as well as infrared (IR) sensors and Hall-effect sensors with associated hardware circuits. The wireless sensing unit consists of three functional modules: the sensing interface, the computational core, and the wireless communication module (Wang et al. 2007). The sensing interface converts analog acceleration signal into digital format and transmits data to the computational core, which consists of an 8-bit Atmel ATmega128 microcontroller and an external Static Random Access Memory (SRAM) chip. Meanwhile, the computational core communicates through a MaxStream 9XCite wireless transceiver with other wireless sensing units and with a central server. In the mobile sensing node, the microcontroller also commands the motors in real time to achieve mobility, based upon real-time motion information provided by the IR sensors and the Hall-effect sensors. The IR sensors detect whether the mobile sensing node is moving inside structural boundary; the Hall-effect sensors monitor the angular velocities of the magnet wheels. Detailed descriptions can be found in Lee et al. (2009) on how to ensure the mobile sensing node moves safely on the underlying structural surface.

The overall weight of the mobile sensing node is about 1 kg (2.2 lbs), most of which is contributed by the magnet wheels, motors, and batteries. Powered by onboard batteries, the mobile sensing node can be completely tetherless during operation. Figure 1 and Figure 2 show that the compliant connection beam is used to attach/detach the accelerometer onto/from the structural surface. When a measurement is to be made, the two cars are driven towards each other to make the compliant beam buckle downwards to the structural surface. With the help of the small magnets fixed around the accelerometer, the accelerometer is firmly attached on the surface, as shown in Figure 1. When the accelerometer is to be detached, the two cars move in opposite directions to lift the accelerometer away from the surface and straighten the compliant beam as shown in Figure 2. When the sensor is attached to the structural surface, the length of the mobile sensing node is 0.191 m (7.5 in). When the sensor is detached, the length of the node is 0.229 m (9 in). The width of the flexonic mobile sensing node is about 0.152 m (6 in), the height is about 0.091m (3.6 in).

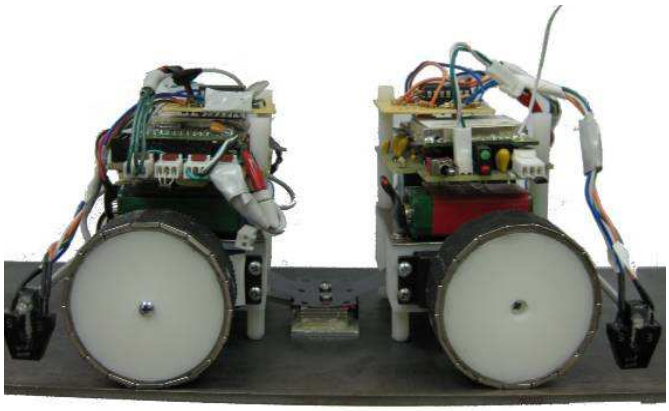

Figure 1. Accelerometer attached to the structure surface.

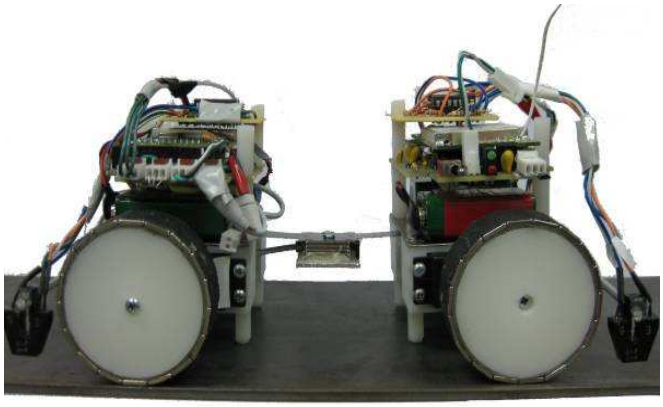

Figure 2. Accelerometer detached from the structure surface.

## 4 DAMAGE DETECTION EXPERIMENTS

This section describes the validation experiments for damage detection using the mobile sensing nodes. Transmissibility function analysis is adopted for processing the mobile sensor data. The experimental setup is introduced first, followed by a description of the data processing procedures. Damage detection results are presented in the end.

### *4.1 Experimental setup*

A 2D laboratory steel portal frame is constructed for exploring structural damage detection using mobile sensing data (Figure 3a). The span of the portal frame is 1.524 m (5 ft), and the height is 0.914 m (3 ft). The beam and two columns have the same rectangular section area of 0.152 m (6 in) × 0.005 m (3/16 in). Hinge connections are adopted at the bases of the two columns. Three acceleration measurement locations are assigned on the left (A1 to A3) and right (A9 to A11) columns, respectively. Five acceleration measurement locations (A4 to A8) are uniformly assigned on the beam (Figure 3b). A steel mass block of 0.575 kg (1.27 lbs) is bonded to the left column, 0.229 m (9 in) above the hinge joint, to simulate a reversible damage. In contrast, the mass of the left column is 4.985 kg (10.99 lbs).

Two mobile sensing nodes are assembled for this group of experiments. The two nodes move to every pair of locations (A1-A2, A2-A3, A3-A4, A4-A5, A5-A6, A6-A7, A7-A8, A8-A9, A9-A10, and A10-A11) in sequence for taking acceleration measurements. Each mobile node carries a Silicon Designs 2260-010 accelerometer. The configuration for the measurement locations A1 and A2 is shown in Figure 4. After the two mobile nodes move to each pair of adjacent measurement locations, they attach the accelerometers onto the steel surface as shown in Figure 1. As shown in Figure 3b, a hammer impact is applied at the middle of these two adjacent measurement locations, so that vibration data can be recorded by the mobile sensing nodes. For example, when the two mobile sensing nodes are at locations A1 and A2, the hammer impact is applied at F1; when the two mobile sensing nodes move to A2 and A3, the hammer impact is applied at F2; and so on. To reduce the effects of experimental uncertainty, measurement at each configuration is repeatedly taken for 20 times. Then the averaged transmissibility function is used for calculating the damage indicator, i.e. number $N$ in Equation (8a) is equal to 20.

### *4.2 Transmissibility analysis to experimental data*

During the experiments, the sampling rate of the mobile sensing nodes is set at 2,500 Hz. Prior to A2D (analog-to-digital) sampling, the accelerometer signal is conditioned by a low-pass fourth-order Bessel filter. After each hammer impact, the vibration decays within about 0.1 second, which is shown in Figure 5. Figure 5a plots the acceleration data at location A1 and Figure 5b plots the acceleration data at location A2; both data sets are simultaneously collected when the hammer hits between A1 and A2.

(a)

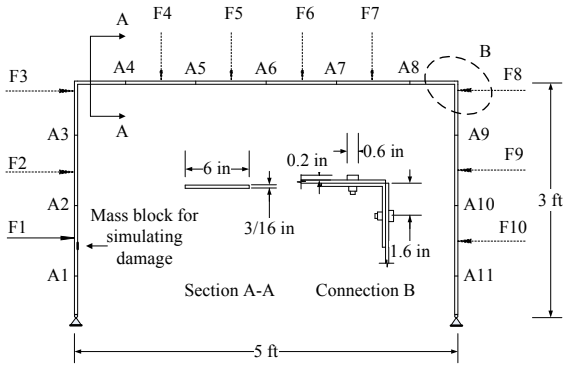


(b)

Figure 3. Laboratory steel portal frame for damage detection using mobile sensing nodes: (a) picture of the portal frame; (b) schematic of sensor and impact locations.

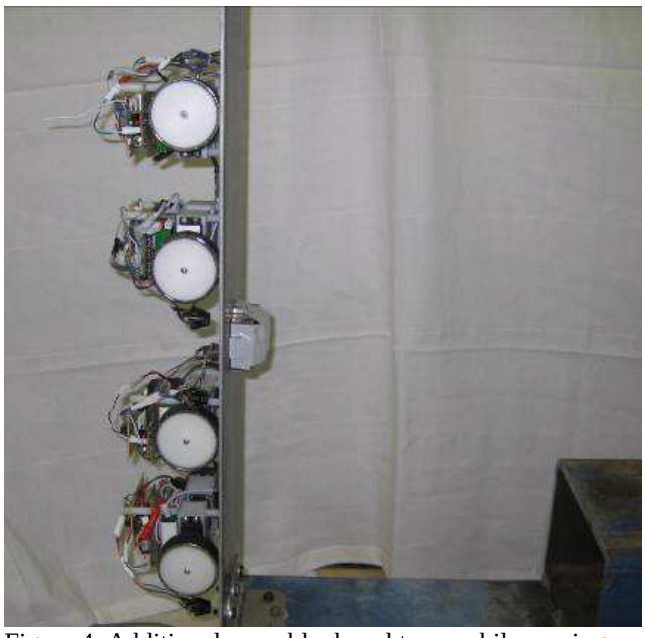

Figure 4. Additional mass block and two mobile sensing nodes, one node allocated at location A1, and the other node at A2 (locations A1 and A2 are as shown in Figure 3).

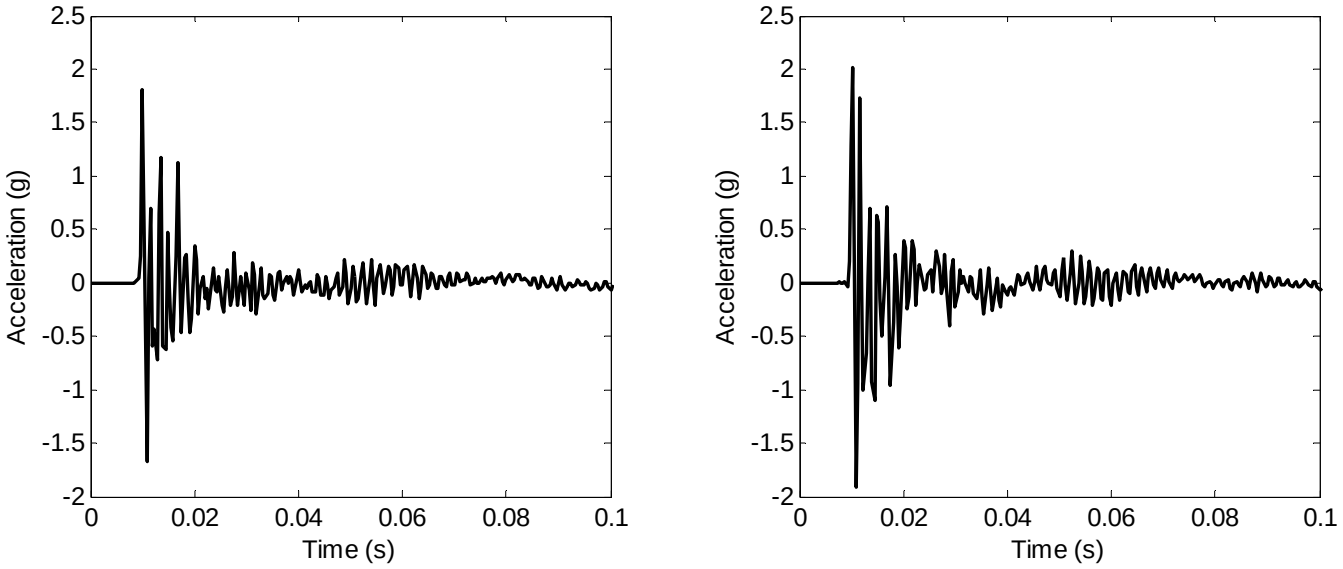


Figure 5. Acceleration data recorded by mobile sensing nodes: (a) location A1; (b) location A2. Hammer impact applied at location F1 (as shown in Figure 3b).

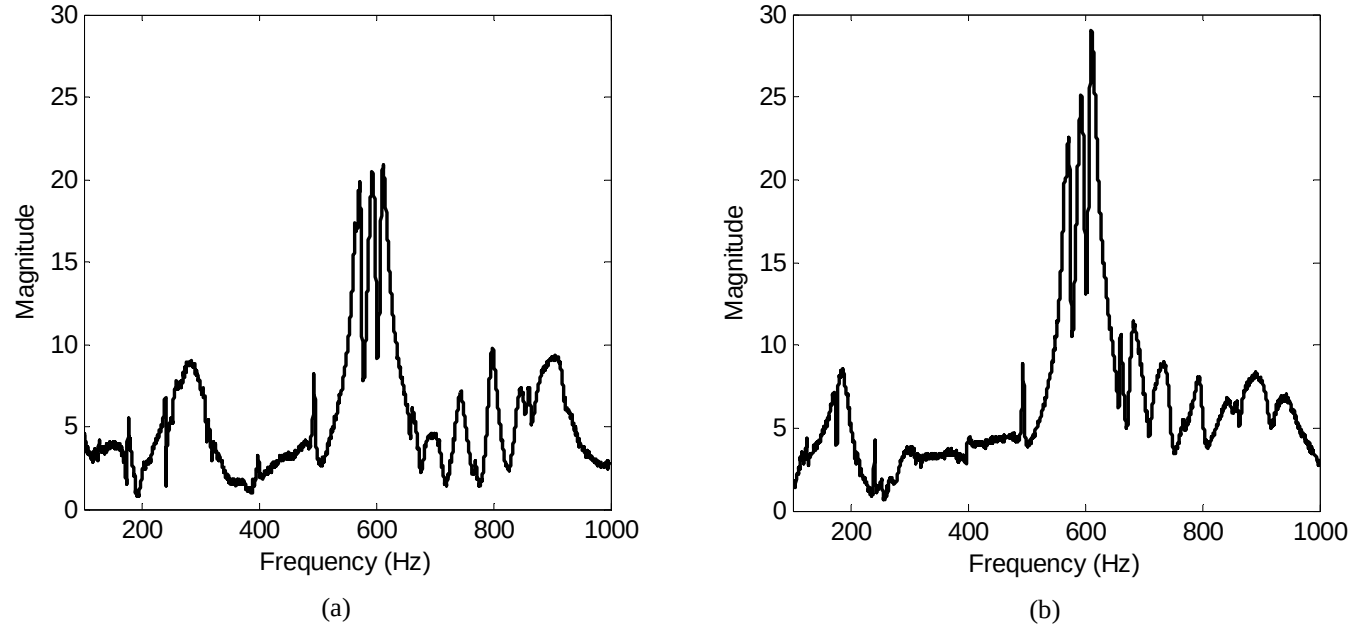


Figure 6. FFT results of the acceleration data collected by the mobile sensing nodes: (a) location A1; (b) location A2.

Figure 6 shows the FFT magnitude of these two acceleration records. Eight-time zero padding is performed to the time history, in order to achieve a frequency resolution of 0.125 Hz in the FFT results.

The 0 - 100 Hz range of the frequency spectra contains many low valleys that are susceptible to sensor noise. According to the definition, transmissibility function is calculated by the ratio between the FFT spectra at two measurement locations. If small numerical values exist near the valleys of the denominator spectrum, the division process results in random peaks in the calculated transmissibility function. These random peaks, consequently, cause the damage indicators to be unreliable. To reduce the sensor noise effect, the 0 - 100 Hz range of the frequency spectra is not used for calculating the transmissibility function. Instead, the 100-1,000 Hz frequency range is used. Accordingly, this frequency range is used for calculating the damage indicator, i.e. $\omega_1$ is set to 100 Hz and $\omega_2$ is set to 1,000 Hz in Equation (7).

As previously mentioned, each hammer impact test is repeated for 20 times, for both undamaged and damaged structures. Figure 7 plots the magnitude of the averaged transmissibility functions of both the undamaged structure and the damaged structure (damage is simulated with an additional mass block). It is shown that the additional mass

block changes the amplitude and peak frequencies of the transmissibility functions. Furthermore, larger difference in the transmissibility functions is observed between location pairs close to the simulated damage location, which is between locations A1 and A2 in Figure 3b. Transmissibility functions at locations far away from the damage generally demonstrate very little change between the undamaged and damaged structures. For example, the difference between the transmissibility functions of the undamaged and damaged structures is relatively large for $T_{1\text{-}2}$, $T_{2\text{-}3}$, and $T_{3\text{-}4}$, and relatively small for $T_{8\text{-}9}$, $T_{9\text{-}10}$, and $T_{10\text{-}11}$.

In addition, the repeatability of the experiments is verified by comparing among the 20 data sets collected from the undamaged structure, as well as from the damaged structure. The objective of the repeatability check is to ensure that experimental uncertainties, including sensor noises and the application of hammer impact, have negligible influence to the damage detection results. Taking the undamaged structure as an example, the 20 acceleration data sets collected for each pair of locations are separated into two groups of 10 data sets. The separation is simply made according to the sequence numbers of each data set, i.e. data sets with odd sequence numbers constitute one group, and data sets with even sequence numbers constitute another group. The averaged transmissibility functions of the two groups (each group containing 10 data sets) are calculated as:

$$T_{ij}^{U\_odd} = \frac{1}{N/2}\sum_{k=1}^{N/2}(T_{ij}^{U})_{2k-1} \tag{9a}$$

$$T_{ij}^{U\_even} = \frac{1}{N/2}\sum_{k=1}^{N/2}(T_{ij}^{U})_{2k} \tag{9b}$$

Figure 8 presents the comparison between the magnitude of $T_{ij}^{U\_odd}$ and $T_{ij}^{U\_even}$. Minor differences exist between the transmissibility functions calculated from different groups of data sets, due to the random nature of physical experiments. Nevertheless, the difference among $T_{ij}^{U\_odd}$ and $T_{ij}^{U\_even}$ is much less than the difference between the transmissibility functions of the undamaged and damaged structures, as shown in Figure 7. The comparison between Figure 7 and Figure 8 confirms the repeatability of the experiments with the undamaged structure. Further repeatability check is conducted among the data sets collected from the damaged structure. A similar level of repeatability is observed as shown in Figure 8. Due to page limit, the repeatability plots using data sets from the damaged structure are not presented in this paper.

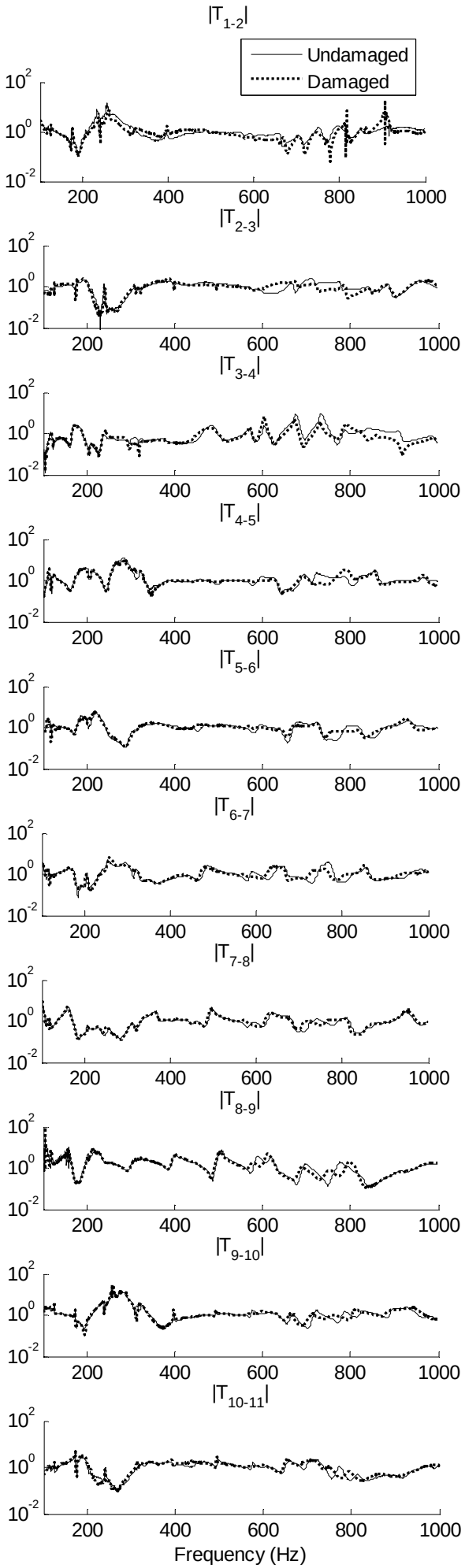


Figure 7. Comparison of transmissibility functions between data sets of the undamaged and damaged structures.

*4.3 Damage detection results*

Following Equation (7), damage indicators are calculated to measure the level of difference between the averaged transmissibility functions of the undamaged structure and of the damaged structure. As presented in Figure 9, the largest damage indicator is $DI_{1\text{-}2}$ = 0.725, which agrees with the correct damage location simulated by the mass block. In general, lower damage indicators are observed for location pairs far away from the damage location.

As a continuation of the repeatability check, the repeatability indicator (*RI*) is defined in parallel to the damage indicator. For example, for the undamaged structure, the repeatability indicator is defined as:

$$RI_{ij}^{U} = \frac{\int_{\omega_1}^{\omega_2} \left| \ln \left| T_{ij}^{U\_odd} \right| - \ln \left| T_{ij}^{U\_even} \right| \right| d\omega}{\int_{\omega_1}^{\omega_2} \left| \ln \left| T_{ij}^{U\_odd} \right| \right| d\omega} \tag{10}$$

Note that using the definition above, a smaller repeatability indicator *RI* represents a higher level of repeatability. Among all the pairs of measurement locations, the largest repeatability indicator for the data sets of the undamaged structure is $RI^{U}_{1\text{-}2}$ =0.1246, as shown in Figure 9. Similarly, the repeatability indicators among the data sets of the damaged structure are also calculated:

$$RI_{ij}^{D} = \frac{\int_{\omega_1}^{\omega_2} \left| \ln \left| T_{ij}^{D\_odd} \right| - \ln \left| T_{ij}^{D\_even} \right| \right| d\omega}{\int_{\omega_1}^{\omega_2} \left| \ln \left| T_{ij}^{D\_odd} \right| \right| d\omega} \tag{11}$$

Among all the pairs of measurement locations, the largest repeatability indicator for the damaged structure is $RI^{D}_{5\text{-}6}$=0.1399. Compared with the damage indicators *DI*, the small values of repeatability indicators $RI^{U}$ and $RI^{D}$ illustrate that the experimental results are reasonably repeatable, and the experimental uncertainties have limited effects to the structural damage detection.

## 5 CONCLUSIONS

This study explores mobile sensors for the damage detection of a laboratory portal frame. Tetherless mobile sensors are developed for autonomous maneuvering upon steel structures, and for automatically attaching/detaching accelerometers onto/from the structure surface. A laboratory portal frame is constructed to validate the capability of the mobile sensors in damage detection. Using acceleration data collected by the mobile sensors, transmissibility function analysis is conducted for identifying a reversible damage simulated by a mass block. In this study, location of the damage can be accurately de-

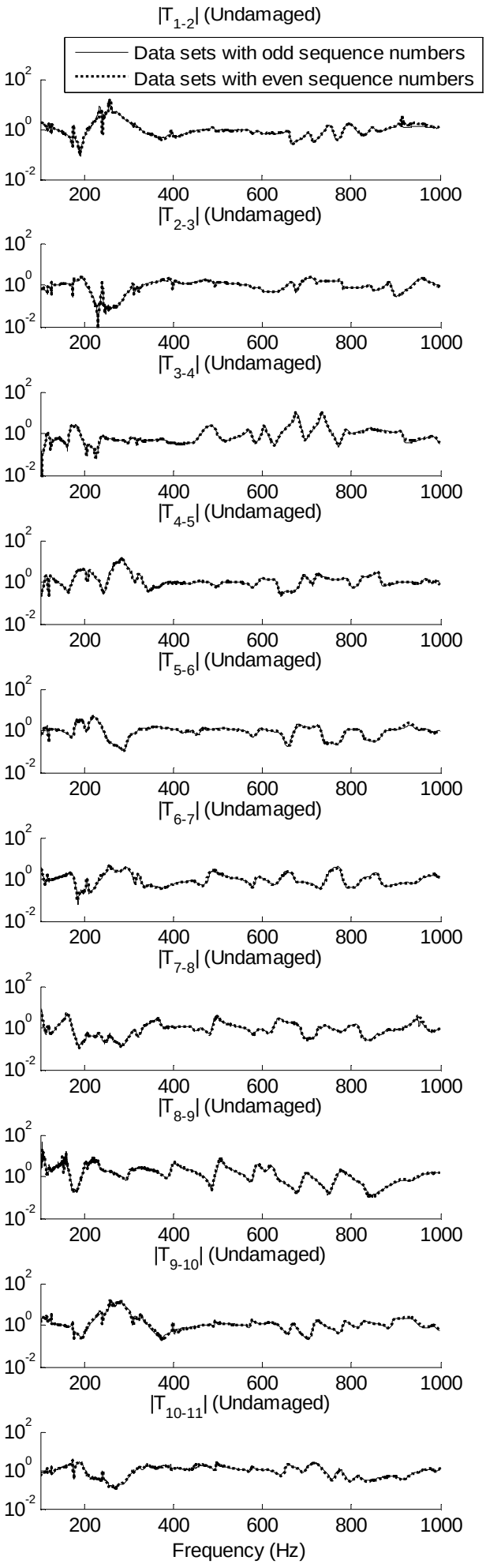


Figure 8. Repeatability of transmissibility functions among data sets for undamaged structure.

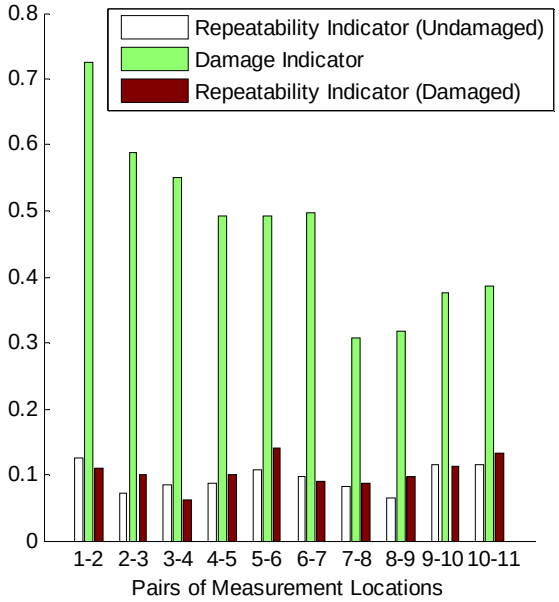


Figure 9. The damage indicators and repeatability indicators for ten pairs of measurement locations.

termined. The advantage of mobile sensors is demonstrated as the high spatial resolution measurement that requires limited number of sensors and little human effort. Such advantage will allow mobile sensor networks bring transformative changes to future practice of structural health monitoring.

Future research will be focused on a number of areas. First, harnessing the embedded computing power of the mobile sensing nodes, research will be conducted to enable the mobile sensing nodes with the capabilities of autonomously detecting potential damages in the structure. In addition, a great amount of efforts will be needed to make the mobile sensing nodes capable of maneuvering upon more realistic structures built with ferromagnetic materials.

## 6 ACKNOWLEDGEMENT

This research is partially sponsored by the National Science Foundation, under grant number CMMI-0928095 (Program Manager: Dr. Shih-Chi Liu). The authors gratefully acknowledge the support.

## 7 REFERENCES

AASHTO. 2008. *Bridging the Gap*. Washington, DC, USA: American Association of State Highway and Transportation Officials.

Akyildiz, I. F., Su, W., Sankarasubramaniam, Y., & Cayirci, E. 2002. A survey on sensor networks. *Communications Magazine, IEEE* 40(8): 102-114.

Devriendt, C. & Guillaume, P. 2008. Identification of modal parameters from transmissibility measurements. *Journal of Sound and Vibration* 314(1-2): 343-356.

Doebling, S. W., Farrar, C. R., & Prime, M. B. 1998. A summary review of vibration-based damage identification methods. *The Shock and Vibration Digest* 30(2): 91-105.

Guo, J., Lee, K.-M., Zhu, D., & Wang, Y. 2009. A flexonic magnetic car for ferro-structural health monitoring. *ASME Dynamic Systems and Control Conference, Hollywood, CA, USA, 12-14 October 2009.*

Johnson, T. J. & Adams, D. E. 2002. Transmissibility as a differential indicator of structural damage. *Journal of Vibration and Acoustics-Transactions of the ASME* 124(4): 634-641.

Johnson, T. J., Brown, R. L., Adams, D. E., & Schiefer, M. 2004. Distributed structural health monitoring with a smart sensor array. *Mechanical Systems and Signal Processing* 18(3): 555-572.

Kess, H. R. & Adams, D. E. 2007. Investigation of operational and environmental variability effects on damage detection algorithms in a woven composite plate. *Mechanical Systems and Signal Processing* 21(6): 2394-2405.

Lee, K.-M., Wang, Y., Zhu, D., Guo, J., & Yi, X. 2009. Flexure-based mechatronic mobile sensors for structure damage detection. *The 7th International Workshop on Structural Health Monitoring, Stanford, CA, USA, 9-11 September 2009.*

Lynch, J. P. & Loh, K. J. 2006. A summary review of wireless sensors and sensor networks for structural health monitoring. *The Shock and Vibration Digest* 38(2): 91-128.

Wang, Y., Lynch, J. P., & Law, K. H. 2007. A wireless structural health monitoring system with multithreaded sensing devices: design and validation. *Structure and Infrastructure Engineering* 3(2): 103-120.

Zhang, H., Schulz, M. J., Ferguson, F., & Pai, P. F. 1999. Structural health monitoring using transmittance functions. *Mechanical Systems and Signal Processing* 13(5): 765-787.